IEEE Access
Multidisciplinary | Rapid Review | Open Access Journal

Received October 23, 2017, accepted December 11, 2017, date of publication December 15, 2017,
date of current version February 14, 2018.

Digital Object Identifier 10.1109/ACCESS.2017.2784094

Design of Broadband Modified Class-J Doherty Power Amplifier With Specific Second Harmonic Terminations

CHAOYI HUANG, SONGBAI HE, (Member, IEEE), AND FEI YOU, (Member, IEEE)
School of Electronic Engineering, University of Electronic Science and Technology of China, Chengdu 611731, China

Corresponding author: Chaoyi Huang (chaoyihuang@foxmail.com)

This work was supported by the National Natural Science Foundation of China under Grant 61571080 and Grant 61271036.

ABSTRACT This paper presents a symmetrical Doherty power amplifier (DPA) based on class-J mode for efficiency enhancement in a broad bandwidth. With a second harmonic suppression integrated into the output matching network of carrier power amplifier (PA) and peaking PA, respectively, the complex interaction of varying second harmonic impedances caused by dynamic load modulation can be eliminated and the second harmonic impedance remains the same reactance at both the output back-off (OBO) region and the saturated power. To meet the requirement of second harmonic termination, the DPA works in conventional class-J mode at the saturated power and a modified class-J continuum is proposed to expand the impedance design space at 8 dB OBO with good efficiency performance. A gallium nitride DPA is designed and fabricated to validate the method over a frequency band of 3.3–3.75 GHz. Under a 10%-duty-cycle pulse excitation, experimental results show the DPA delivers 48-48.8 dBm output power with a drain efficiency (DE) of 58%–71%. At 8 dB OBO, a measured DE of 44%–55% is achieved with a gain of 11.8–13.5 dB. When driven by a 2-carrier 40-MHz long-term evolution signal with a peak-to-average power ratio of 8 dB, the DPA exhibits an adjacent channel leakage ratio of −30 dBc at an average output power of 40.7 dBm at 3.45 GHz.

INDEX TERMS Doherty power amplifiers (DPAs), class-J, broadband, high efficiency, the fifth generation (5G).

I. INTRODUCTION

With the explosive growth of mobile devices, the fifth generation of mobile communication systems (5G) is expected to be standardized and commercialized towards the year 2020 and beyond [1]. According to new standards in 5G, the ever-increasing demand for large user experience data rate leads to wide signal bandwidth and high peak-to-average power ratio (PAPR). In this case, the power amplifier (PA), as a crucial element of the transmitter, requires efficiency enhancement at the output back-off (OBO) region over a wide frequency band. Facing this challenge, several PA architectures to handle high PAPR have been presented such as envelope tracking (ET) [2], Doherty [3], linear amplification with nonlinear components (LINC) [4] and envelope elimination and restoration (EER) [5]. Among these candidate techniques, the Doherty PA (DPA) is widely used in the base-station system on account of its simple circuit structure [6], [7]. The DPA can achieve high efficiency at both the OBO region and the saturated power by dynamic load modulation. However, the quarter-wavelength impedance inverter, which realizes the optimum impedance transformation only at a certain frequency, limits the bandwidth of the conventional DPA.

Recently, various solutions have been proposed to improve the bandwidth of the DPA. In [8] and [9], low-order impedance inverters are adopted to replace the quarter-wave length transmission lines to extend the bandwidth. The works of [10] and [11] achieve wideband DPAs employing the post-matching network (PMN) to reduce the impedance transformation ratio. A DPA exploiting an integrated compensating reactance for broadband operation is introduced in [12]. Moreover, to obtain wideband behavior, a comprehensive method via real frequency technique is presented in [13] and the output matching networks are implemented using wideband compensators [14].

For the DPA, the dynamic load modulation leads to a complex interaction between the carrier PA and the peaking PA, which means the fundamental and harmonic impedances

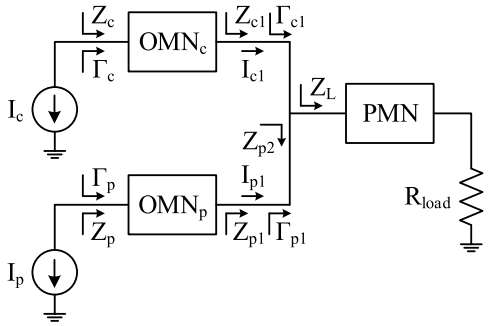

FIGURE 1. Simplified circuit diagram of the conventional DPA with PMN.

simultaneously change at the combining point in the DPA. It is noteworthy that previously published papers about the DPA [15]–[18] mainly focus on the fundamental impedance, while ignoring the effect of harmonic components.

In fact, tuning harmonic loads can avoid the overlap between current and voltage waveforms so as to decrease the power dissipation within the transistor, such as class-F mode [19] and inverse class-F mode [20]. Furthermore, harmonic manipulation has been utilized to extend the bandwidth in continuous PA modes [21]–[26]. For instance, the class-J mode described in [21], maintains the same efficiency and power performance as class-B mode over a wide range of second harmonic terminations, representing an extension to design space, therefore, it is a suitable solution to realize broadband PAs.

In this paper, the effect on the second harmonic component due to the dynamic load modulation is eliminated by adding a second harmonic suppression into the output matching network (OMN), resulting in a fixed second harmonic reactance at both the OBO region and the saturated power. Therefore, the second harmonic termination can be set in line with the conventional class-J mode and the carrier PA may be considered as a conventional class-J PA at the saturated power. When the peaking PA is off, a modified class-J mode is presented to realize an 8 dB OBO with a symmetrical architecture. The modified class-J mode significantly expands the impedance design space at the low power which indicates a more available design freedom. To validate the proposed theory, a broadband DPA for the base station in 5G is designed, fabricated and experimentally verified.

This paper is organized as follows. The dynamic load modulation is analyzed and the specific second harmonic termination is determined in Section II. Section III introduces the detailed theoretical derivation of modified class-J mode. The circuit of the proposed DPA is designed and simulated in Section IV. Section V presents the measurement results under pulse signal excitation as well as under modulated signal excitation. Finally, the conclusion is given in Section VI.

II. SPECIFIC SECOND HARMONIC TERMINATIONS

A conventional DPA usually consists of two PAs, the carrier PA biased for class-B operation and the peaking PA biased for class-C operation. The PMN, providing an appropriate fundamental load termination, has been widely used to extend the bandwidth of the DPA. The simplified circuit diagram of the conventional DPA with PMN is shown in Fig. 1. Each transistor is assumed to be an ideal current generator. The OMN of the carrier PA (OMN_c) and the OMN of the peaking PA (OMN_p) are responsible for impedance transformation. Z_L represents the combining load which is always transformed from a 50-Ω load by the PMN. Based on the active load modulation, the effective load impedances of the carrier and peaking branches are described as follows

$$Z_{c1} = \begin{cases} Z_L(1+\dfrac{I_{p1}}{I_{c1}}) = Z_L(1+\alpha) & 0 \le OBO < \beta \\ Z_L & \beta \le OBO \end{cases} \quad (1)$$

$$Z_{p1} = Z_L(1+\frac{I_{c1}}{I_{p1}}) = Z_L(1+\frac{1}{\alpha})\ 0 \le OBO < \beta \quad (2)$$

where β is the value of the OBO level at the low power, which means the peaking PA just shuts down and the output impedance of the peaking branch becomes infinite ($Z_{p2} = \infty$) at β dB OBO. α is the current ratio between the peaking branch and the carrier branch (I_{p1} and I_{c1} are in-phase components under the ideal Doherty operation) and is defined as

$$\alpha = \frac{I_{p1}}{I_{c1}}. \quad (3)$$

To analyze the effect of load modulation on the impedance at the current-generator plane, scattering parameters are used to express the OMNs and the scattering matrix of OMN_c is given by

$$S_c = \begin{bmatrix} S_{11}^c & S_{12}^c \\ S_{21}^c & S_{22}^c \end{bmatrix} = \begin{bmatrix} 0 & e^{j\theta} \\ e^{j\theta} & 0 \end{bmatrix} \quad (4)$$

where θ is the phase of S_{21}^c in the lossless network. According to the theory of power waves [27], the load reflection coefficient of the OMN_c is given by

$$\Gamma_{c1} = \frac{Z_{c1} - Z_L^*}{Z_{c1} + Z_L}. \quad (5)$$

The input reflection coefficient of the OMN_c can be written as

$$\Gamma_c = S_{11}^c + \frac{S_{12}^c S_{21}^c}{1 - S_{22}^c \Gamma_{c1}} \Gamma_{c1} = \Gamma_{c1} e^{j2\theta}. \quad (6)$$

Z_L is always set to be resistive load at fundamental frequencies ($Z_{L,f} = R_1$) by the PMN. The OMN_c is assumed to realize the fundamental impedance matching at the low power (β dB OBO). Thus, by replacing (1) in (5), the load reflection coefficient of the OMN_c at the saturated power can be established

$$\Gamma_{c1,sat,f} = \frac{R_1(1+\alpha_{sat,f}) - R_1}{R_1(1+\alpha_{sat,f}) + R_1} = \frac{\alpha_{sat,f}}{2+\alpha_{sat,f}}. \quad (7)$$

From (6) and (7), the input reflection coefficient of the OMN_c at the saturated power can be derived as

$$\Gamma_{c,sat,f} = \frac{\alpha_{sat,f}}{2+\alpha_{sat,f}} e^{j2\theta}. \quad (8)$$

Hence, the fundamental impedance of the carrier PA at the saturated power ($Z_{c,sat,f}$) is located on the circle with constant reflection coefficient magnitude ($|\Gamma_{c,sat,f}| = \alpha_{sat,f}/(2+\alpha_{sat,f})$) in the smith chart.

As mentioned above, harmonic terminations play an important role on efficiency. The simulated efficiency and output power contours for second and third harmonic load-pulls employing Wolfspeed's CGHV27030S GaN HEMT at 3.4 GHz are shown in Fig. 2. From the results, we can see that the second harmonic termination significantly affects the performance and the third harmonic termination has little effect on efficiency and output power, so it is necessary to control the second harmonic impedance.

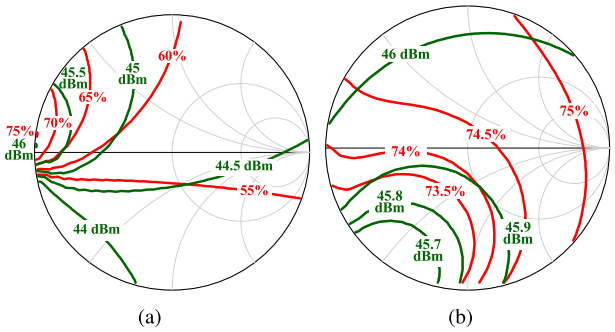

FIGURE 2. Simulated efficiency (red lines) and output power (green lines) contours at 3.4 GHz. (a) Second harmonic load-pull. (b) Third harmonic load-pull.

When considering the harmonic component, Z_L will be complex-valued and frequency-dependent at harmonic frequencies because of the characteristic of the PMN. For example, at a certain second harmonic frequency ($2f_0$), Z_L is a complex impedance ($Z_{L,2f_0} = R_{2f_0} + jX_{2f_0}$), and the load reflection coefficient at second harmonic frequencies can be written as

$$\Gamma_{c1,2f} = \frac{Z_{c1,2f} - R_{2f_0} + jX_{2f_0}}{Z_{c1,2f} + R_{2f_0} + jX_{2f_0}}. \tag{9}$$

It is obvious that $|\Gamma_{c1,2f}|$ changes with frequency, which leads to an irregular variation on the second harmonic impedance of the carrier PA ($Z_{c,2f}$). Therefore, it is difficult to find an OMN to achieve the impedance transformation at fundamental and harmonic frequencies simultaneously.

To overcome this restriction, second harmonic suppressions are integrated into the OMN_c and OMN_p, respectively, as shown in Fig. 3. $Z_{sc,2f}$ and $Z_{sp,2f}$ denote the output impedances of the second harmonic suppression networks (SHSNs) at second harmonic frequencies. $Z_{c2,2f}$ and $Z_{p4,2f}$ are the second harmonic loads of second harmonic matching networks (SHMNs). Since transmission zeros distribute at second harmonic frequencies, $Z_{sc,2f}$ and $Z_{sp,2f}$ are equal to zero. The SHSNs and the rest of the OMNs are connected in parallel, so $Z_{c2,2f}$ and $Z_{p4,2f}$ will also equal zero. This indicates the load modulation for the second harmonic component can not impact on the values of $Z_{c2,2f}$ and $Z_{p4,2f}$. In other words, the load modulation just needs to be given

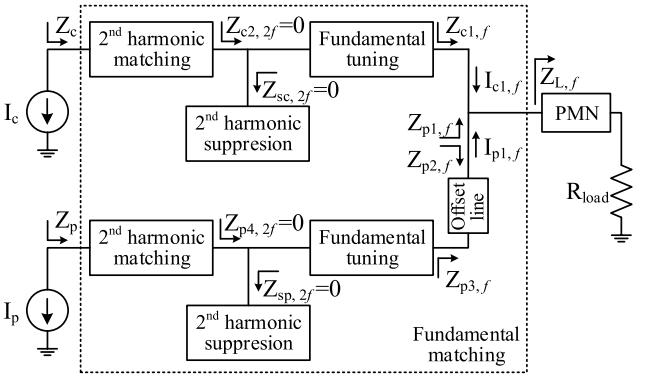

FIGURE 3. Simplified circuit diagram of the proposed DPA.

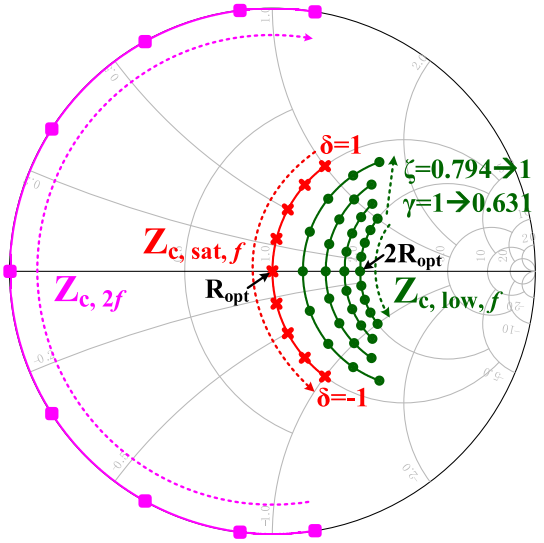

FIGURE 4. Impedance design space of the carrier PA at the current-generator plane (normalized to R_{opt}).

consideration on the fundamental component. Moreover, the second harmonic terminations at the current-generator plane ($Z_{c,2f}$ and $Z_{p,2f}$) are only dependent on the SHMNs.

The SHMNs are supposed to be passive and lossless, then $Z_{c,2f}$ and $Z_{p,2f}$ transformed from zero by the SHMNs will be purely reactive, which is easy to associate with class-J PA. If the carrier PA works in class-J mode at the saturated power, the fundamental and second harmonic terminations at the current-generator plane have been analyzed in [21] and are given by

$$Z_{c,sat,f} = R_{opt} + j\delta R_{opt} \quad -1 \le \delta \le 1 \tag{10}$$

$$Z_{c,sat,2f} = -j\frac{3\pi}{8}\delta R_{opt} \quad -1 \le \delta \le 1 \tag{11}$$

where R_{opt} is the optimal impedance for running the Class-B operation at the saturated power. As $Z_{c,2f}$ remains unaffected by load modulation, the specific second harmonic terminations can be obtained in (12) and are shown in Fig. 4.

$$Z_{c,2f} = Z_{c,low,2f} = Z_{c,sat,2f} = -j\frac{3\pi}{8}\delta R_{opt} \quad -1 \le \delta \le 1. \tag{12}$$

III. MODIFIED CLASS-J MODE AT THE LOW POWER

According to the theory of Doherty PA, a conventional symmetrical DPA ($\alpha_{sat,f} = 1$) has a β of 6 dB with the same performance of class-B PA and an asymmetrical DPA ($\alpha_{sat,f} > 1$) is usually used to achieve a larger β. In this section, based on the specific second harmonic terminations stated in the former section, a modified class-J mode at the low power is presented to extend the OBO region and impedance design space with a symmetrical configuration.

At the low power, the peaking PA is off, so the max current swing of the carrier PA attains half-maximum value. The current waveform of the carrier PA then becomes

$$i_{c,low}(\theta) = \frac{\zeta}{2} I_{\max}\left(\frac{1}{\pi} + \frac{1}{2}\cos\theta + \frac{2}{3\pi}\cos 2\theta \ldots\right) \quad (13)$$

where $0 \le \zeta \le 1$ is the coefficient determined the amplitude of the current, and $I_{\max}$ is the maximum current amplitude at the saturated power.

The voltage waveform of the conventional class-J mode is described as follows [21]

$$v_J(\theta) = V_{DD}(1 - \cos\theta)(1 - \delta\sin\theta) \quad -1 \le \delta \le 1 \quad (14)$$

where V_{DD} is the drain bias voltage. Through (13) and (14), the fundamental and the second harmonic terminations at the low power for class-J mode can be derived as follows

$$Z_{J,low,f} = \frac{2}{\zeta} R_{opt}(1 + j\delta) \quad 0 \le \zeta \le 1 \quad (15)$$

$$Z_{J,low,2f} = -j\frac{3\pi}{4\zeta}\delta R_{opt} \quad 0 \le \zeta \le 1 \quad (16)$$

where $R_{opt} = 2V_{DD}/I_{\max}$ is the class-B loadline resistance at the saturated power. Since $Z_{c,2f}$ has been determined in (12), $-\zeta/2 \le \delta \le \zeta/2$ is obtained by equating (12) and (16).

The fundamental output powers at the saturated power and the low power for class-J mode can be calculated as

$$P_{c,sat,f} = \frac{1}{4} I_{\max} V_{DD} \quad (17)$$

$$P_{J,low,f} = \frac{\zeta}{8} I_{\max} V_{DD}. \quad (18)$$

Subsequently, the value of β for conventional class-J mode is given by

$$\beta_J = \left|10\log\left(\frac{P_{J,low,f}}{2P_{c,sat,f}}\right)\right| = 6 + |10\log(\zeta)|. \quad (19)$$

As can be seen from (19), β_J is equal to 6 dB when $\zeta = 1$. Furthermore, β_J increases over 6 dB with the reduction of ζ, but $\mathrm{Re}\left[Z_{J,low,f}\right]$ will also be larger than $2R_{opt}$. For a β_J of 8 dB, $\mathrm{Re}\left[Z_{J,low,f}\right] = 3.17R_{opt}$ can be evaluated via (15) and (19), resulting in an increase on the impedance transformation ratio, which makes it difficult to be realized by a simple OMN.

A coefficient $\gamma \in (0, 1]$ is adopted to adjust the fundamental impedance at the low power ($Z_{c,low,f}$) to satisfy the condition of $\mathrm{Re}\left[Z_{c,low,f}\right] \le 2R_{opt}$. For $\zeta = 1$, $i_{c,low}(\theta)$ reaches its max amplitude, meanwhile a modified voltage waveform is defined in (20) to keep the voltage above zero.

$$v_{low}(\theta) = V_{DD}(1 - \gamma\cos\theta)(1 - \delta\sin\theta) \; at \; \zeta = 1. \quad (20)$$

By combining (13) and (20), $Z_{c,low,f}$ and the second terminations at the low power ($Z_{c,low,2f}$) can be expressed as

$$Z_{c,low,f} = 2R_{opt}(\gamma + j\delta) \quad 0 < \gamma \le 1 \quad (21)$$

$$Z_{c,low,2f} = -j\frac{3\pi}{4}\gamma\delta R_{opt} \quad 0 < \gamma \le 1. \quad (22)$$

Considering $Z_{c,2f}$ described in (12), the relationship between γ and δ can be computed by equating (12) and (22) as follows

$$-\frac{1}{2\gamma} \le \delta \le \frac{1}{2\gamma}. \quad (23)$$

When $0 \le \zeta \le 1$, using (13) and (21), the output power at the low power can be derived as

$$P_{c,low,f} = \frac{\zeta^2\gamma}{16} I_{\max}^2 R_{opt} = \frac{\zeta^2\gamma}{8} V_{DD} I_{\max}. \quad (24)$$

Then, the drain efficiency (DE) at the low power is given by

$$\eta_{low} = \frac{P_{c,low,f}}{P_{DC,low}} = \frac{\frac{\zeta^2\gamma}{8} V_{DD} I_{\max}}{\frac{\zeta}{2\pi} V_{DD} I_{\max}} = \frac{\pi}{4}\zeta\gamma. \quad (25)$$

According to (17) and (24), β can be calculated as

$$\beta = \left|10\log\left(\frac{P_{c,low,f}}{2P_{c,sat,f}}\right)\right| = 6 + \left|10\log(\zeta^2\gamma)\right|. \quad (26)$$

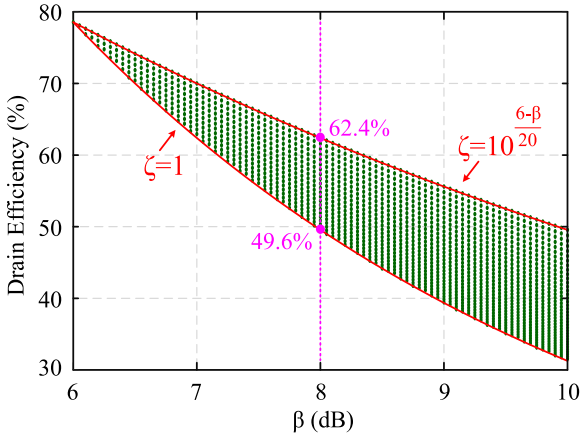

FIGURE 5. Theoretical drain efficiency versus β.

Since η_{low} and β are both found, the relationship between them may be evaluated in (27) via (25) and (26), and the result is shown in Fig. 5.

$$\begin{cases} \beta \ge 6 \\ 10^{\frac{6-\beta}{20}} \le \zeta \le 1 \\ \eta_{low} = \frac{10^{\frac{6-\beta}{10}}}{\zeta}\frac{\pi}{4}. \end{cases} \quad (27)$$

Note that from the result, the modified class-J mode can achieve an efficiency above 49.6% at 8 dB OBO. If β is set

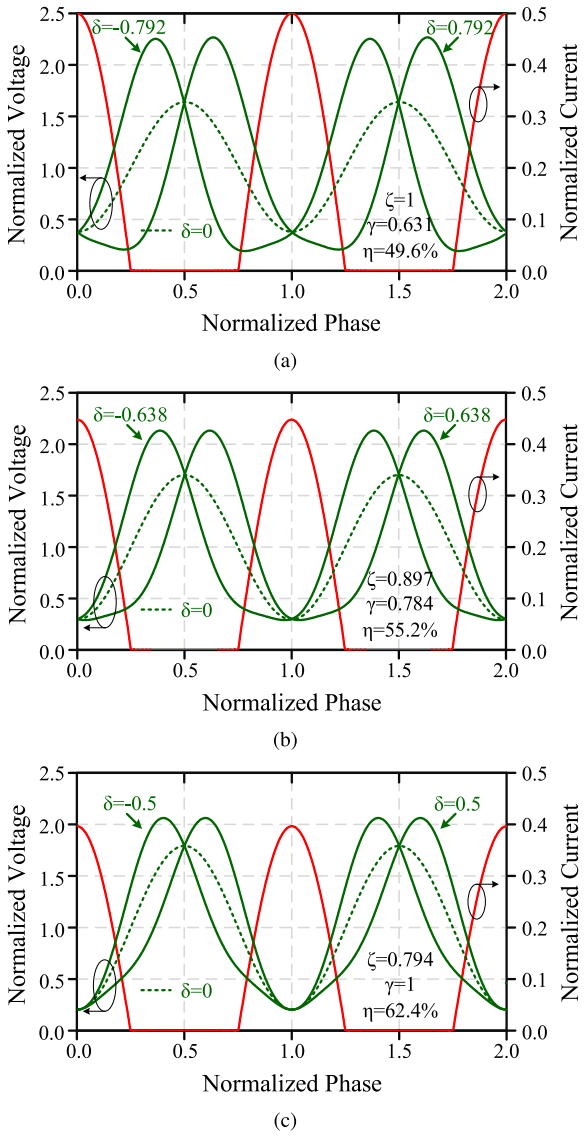

FIGURE 6. Current (normalized to I_{max}) and voltage (normalized to V_{DD}) waveforms at the carrier current-generator plane when $\beta = 8$ *dB*. (a) For $\zeta = 1$. (b) For $\zeta = 0.897$. (c) For $\zeta = 0.794$.

equal to 8 dB, according to (21), (22), (26) and (27), the related conditions can be derived in the following formulas:

$$\begin{cases} 0.794 \le \zeta \le 1 \\ 0.631 \le \gamma = \dfrac{0.631}{\zeta^2} \le 1 \\ -\dfrac{1}{2\gamma} \le \delta \le \dfrac{1}{2\gamma} \\ Z_{c,low,f} = 2R_{opt}(\gamma + j\delta) \\ Z_{c,2f} = Z_{c,low,2f} = -j\frac{3\pi}{4}\gamma\delta R_{opt}. \end{cases} \tag{28}$$

The above formulas describe a set of viable terminations for a β of 8 dB which are shown in Fig. 4, meanwhile the current (normalized to $I_{\max}$) and the voltage (normalized to V_{DD}) waveforms at the carrier current-generator plane are plotted in Fig. 6. It can be observed that, a significantly wider impedance design space is provided by the symmetrical Doherty PA with modified class-J mode at 8 dB OBO, which indicates an increased flexibility in the OMN design.

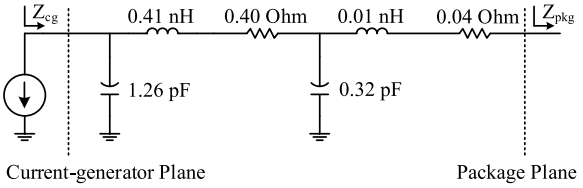

FIGURE 7. Equivalent package parasitic model of CGHV27030S with frequencies ranging from 3.3 GHz to 7.6 GHz.

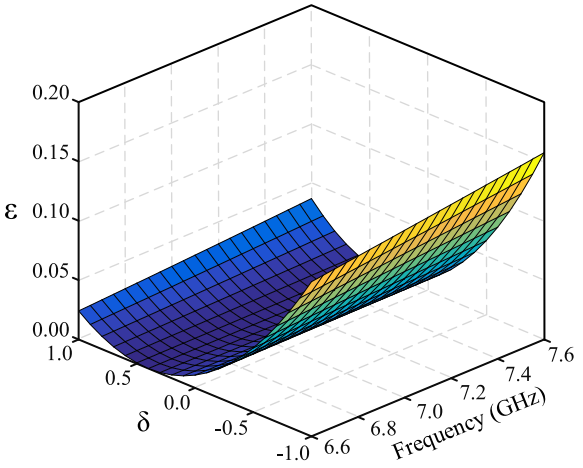

FIGURE 8. ε at the second harmonic frequencies.

IV. BROADBAND SYMMETRICAL DPA IMPLEMENTATION

Recently, 5G has become a focal point for global research and development. According to the spectrum planning, frequencies below 6 GHz are still the primary bands of 5G due to their good propagation characteristics. Considering the spectrum resource, a symmetrical DPA for the base station in 5G is designed to operate over a frequency band of 3.3-3.8 GHz with a saturated power above 48 dBm. Two Wolfspeed's CGHV27030S GaN HEMTs are used to demonstrate the design on a 20-mil RO4350B substrate. V_{DD} is set as 50 V, then $I_{\max} = 2.53\,A$ can be calculated through (17), thus R_{opt} will be 39.5 Ω.

A. IMPEDANCE DESIGN SPACE AT THE PACKAGE PLANE

The impedance design spaces analyzed in Section II and III are at the current-generator plane, and consequently the package parasitics of the device need to be de-embedded. An approximated equivalent parasitic network for Wolfspeed's CGH40010F GaN HEMT has been presented in [28]. Similarly, the package parasitic model of the selected transistor can be extracted with frequencies ranging from 3.3 GHz to 7.6 GHz, as shown in Fig. 7.

The package parasitic network can be expressed in terms of the ABCD matrix, subsequently, the impedance at the

TABLE 1. Transformation of $Z_{c,2f}$ at 6.6 GHz.

δ	$Z_{c,2f}$	Z_{pkg}
-1	$j46.53$	$-0.48-j4.28$
0	0	$-0.71-j22.68$
1	$-j46.53$	$-0.32+j12.17$

TABLE 2. Transformation of $Imag\left[Z_{pkg}\right]$ at 6.6 GHz.

δ	$Imag\left[Z_{pkg}\right]$	Z_{cg}
-1	$-j4.28$	$5.15+j46.16$
0	$-j22.68$	0.42
1	$j12.17$	$0.95-j46.50$

current-generator plane can be transferred to the package plane with the following formula:

$$Z_{pkg}=\frac{B-DZ_{cg}}{CZ_{cg}-A}. \tag{29}$$

$Z_{c,2f}$ described in (12) is a continuum of pure reactances at the current-generator plane, when it performs the transformation given in (29), there will be negative real parts due to the resistors in the package parasitic model. The negative $\mathrm{Re}\left[Z_{pkg}\right]$ can not be achieved by a passive and lossless SHMN. Table 1 shows an example of the situation at 6.6 GHz. Note that the absolute value of $\mathrm{Re}\left[Z_{pkg}\right]$ is minuscule compared to R_{opt}, we may just take $\mathrm{Imag}\left[Z_{pkg}\right]$ as the second harmonic impedance design space and then transfer $\mathrm{Imag}\left[Z_{pkg}\right]$ back to the current-generation plane via (30), as shown in Table 2.

$$Z_{cg}=\frac{AZ_{pkg}+B}{CZ_{pkg}+D}. \tag{30}$$

In this case, $\mathrm{Re}\left[Z_{cg}\right]$ is also minuscule compared to R_{opt} and $\mathrm{Imag}\left[Z_{cg}\right]$ is close to $Z_{c,2f}$. ε is defined to denote the ratio between $\mathrm{Re}\left[Z_{cg}\right]$ and R_{opt}, as shown in Fig. 8. According to the effect of ε on efficiency elaborated in [29], ε with a maximum value of 0.16 in this design will lead to an efficiency reduction of less than 2%, which is completely acceptable.

Fig. 9 shows the impedance design space of the carrier PA at the package plane. The available impedances are widely distributed and bring about multiple choices on the corresponding values of fundamental and second harmonic components.

B. CIRCUIT SIMULATION

The impedance design space at the package plane shown in the previous subsection gives the design goal for the OMN. A microstrip radial stub is adopted to realize the second harmonic suppression. Subsequently, the SHMN can be synthesized to implement the second harmonic impedance

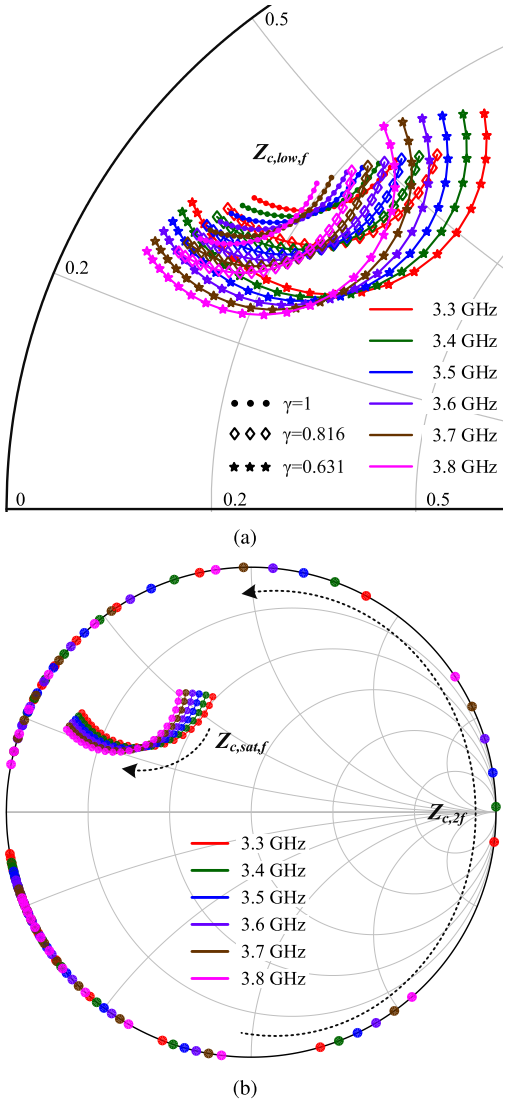

FIGURE 9. Impedance design space of the carrier PA at the package plane (normalized to 50 Ω). (a) At the low power ($\beta = 8$ *dB*). (b) At the saturated power.

transformation from short-circuit point to the optimum area. The SHMN and the SHSN are not only related to the second harmonic component but also a part of the fundamental matching network. As the SHMN and the SHSN have been determined, two stepped transmission lines are added behind the SHSN for fundamental tuning.

According to (28), the turning-on point of the peaking PA depends on ζ. Since $\zeta \in [0.794, 1]$, the corresponding input power has a range of 2 dB, leading to different turning-on points of the peaking PA in a wide bandwidth. It is an indeed difficult goal to achieve with an even splitter and a broadband class-C peaking PA. In order to facilitate the implementation, the turning-on point of the peaking PA is set with the same as the conventional symmetrical DPA ($\zeta = 1$) within the target bandwidth.

Considering the peaking PA is off when $\zeta \leq 1$, it will not affect the analysis in section III, which means the novel

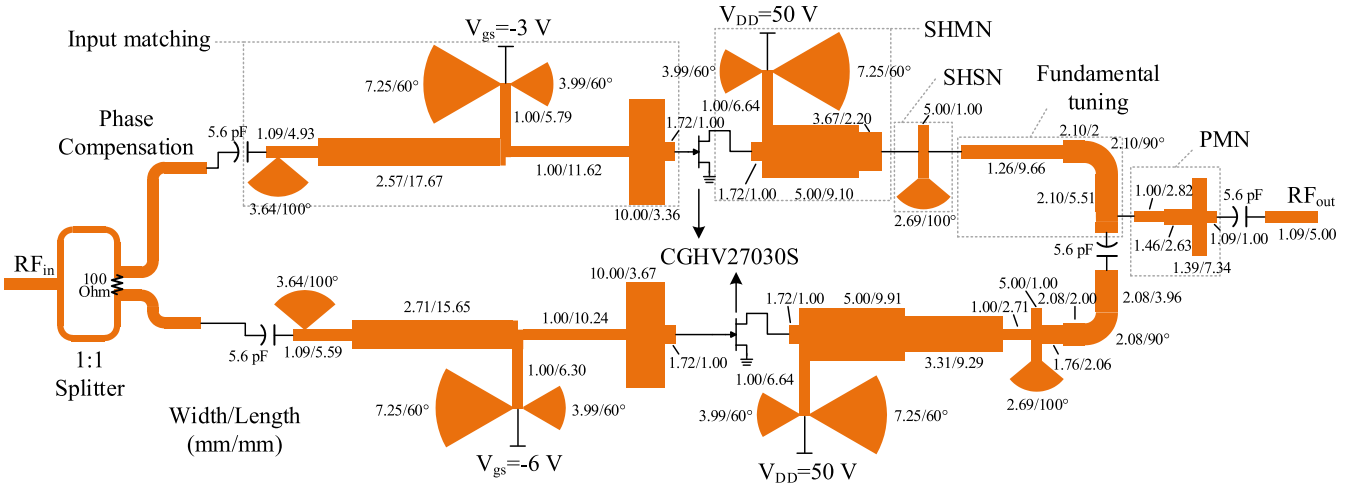

FIGURE 10. Schematic diagram of the proposed DPA.

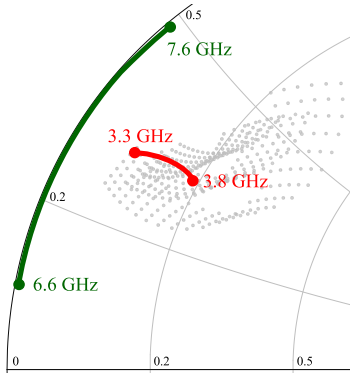

FIGURE 11. Simulated impedances of the carrier PA at the package plane at the low power.

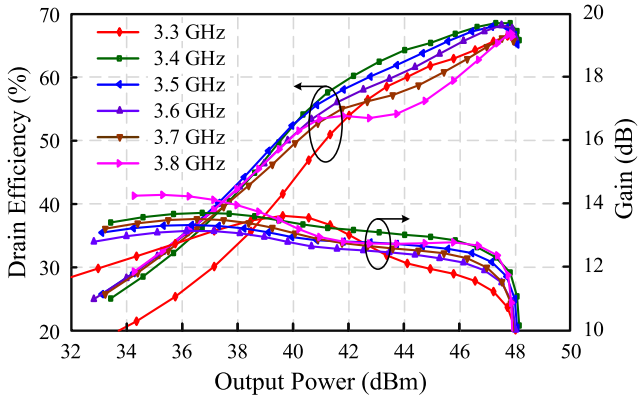

FIGURE 12. Simulated DE and gain versus output power.

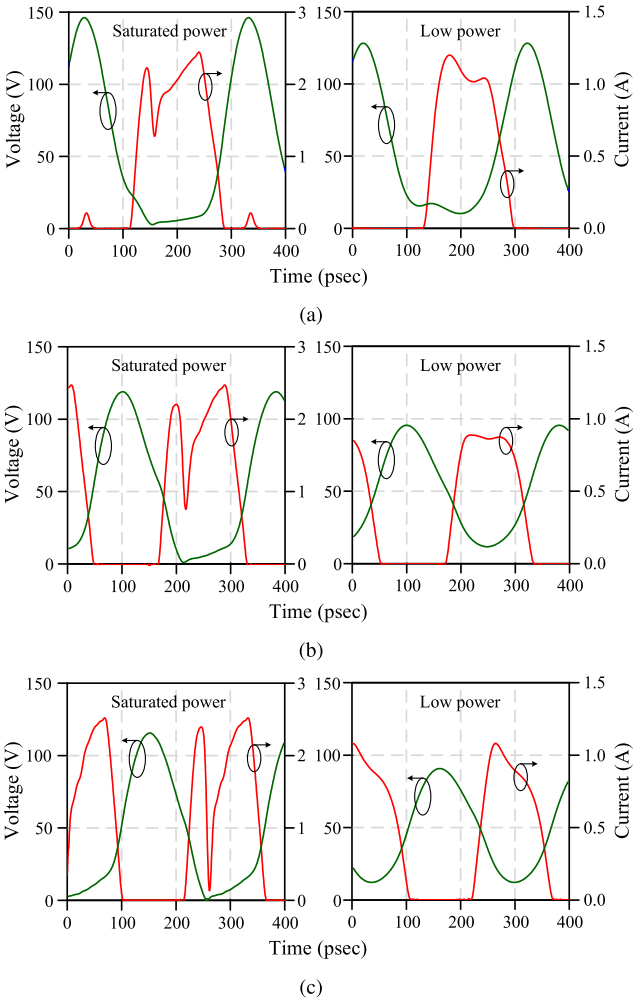

FIGURE 13. Simulated drain current and voltage waveforms. (a) At 3.3 GHz. (b) At 3.55 GHz. (c) At 3.8 GHz.

design space is adequate under the bias condition. In this case, the DPA will reach the first efficiency peak between 6-8 dB OBO which is decided by the choice of the impedances. For illustration, the first efficiency peak will appear at 6 dB OBO and 8 dB OBO, respectively when $\gamma = 1$ and $\gamma = 0.631$. Regardless of where the first efficiency peak appears, the DE keeps higher than 49.6% at 8 dB OBO based on the proposed theory.

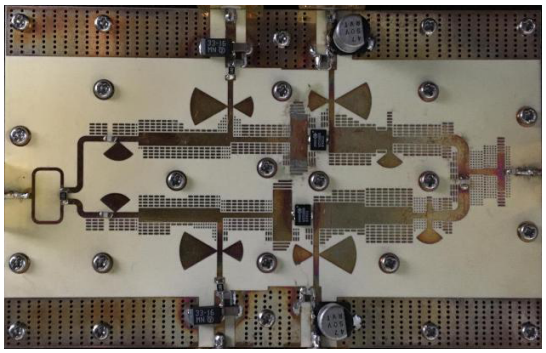

FIGURE 14. Photograph of the fabricated DPA.

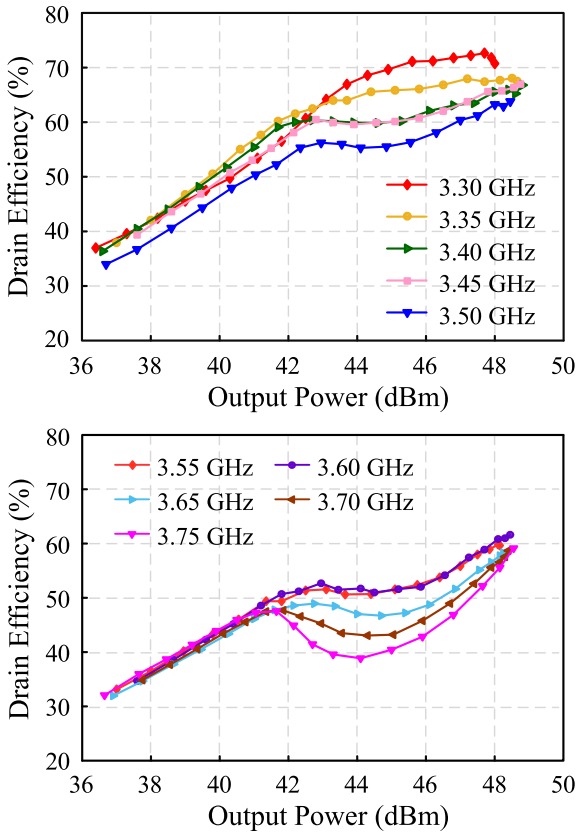

FIGURE 15. Measured DE versus output power.

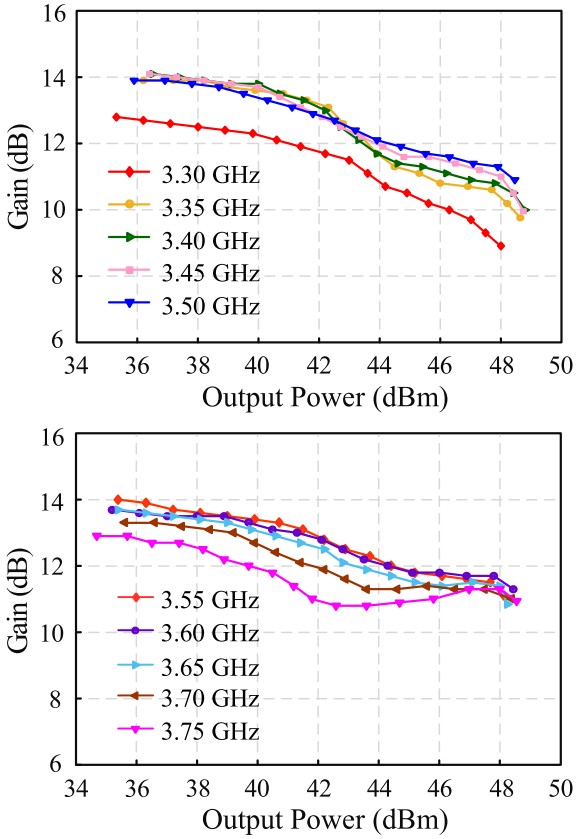

FIGURE 16. Measured gain versus output power.

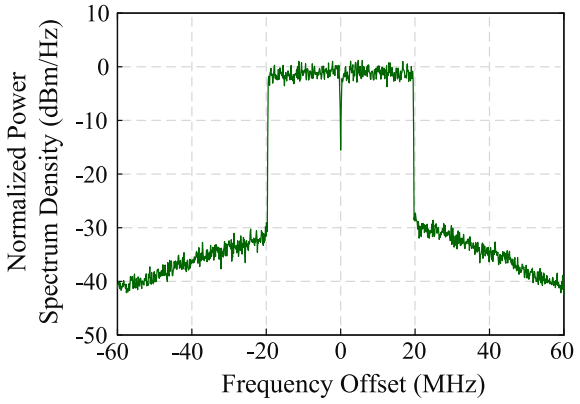

FIGURE 17. Measured spectrum with a 2-carrier 40-MHz LTE signal at 3.45 GHz.

The complete schematic diagram of the proposed DPA is shown in Fig. 10. The carrier PA is biased at $V_{gs} = -3\ V$, while the peaking PA is biased at $V_{gs} = -6\ V$. Fig. 11 exhibits a satisfactory impedance matching of the carrier PA at the package plane when $\beta = 8\ dB$.

Fig. 12 shows the simulated DE and gain of the proposed DPA versus output power. The DPA achieves a DE of higher than 44% at 8 dB OBO with a saturated power of about 48 dBm across a frequency band of 3.3-3.8 GHz. Meanwhile, the gain ranges from 12.8 dB to 13.7 dB at 8 dB OBO.

To validate the operation mode of the proposed DPA, the simulated drain current and voltage waveforms are plotted in Fig. 13. At the saturated power, the waveforms are quite similar to the conventional class-J mode. Moreover, the minor amplitudes of the voltage waveforms at the low power are in conformity with the analysis of the modified class-J mode in Section III.

V. MEASURED RESULTS

A photograph of the fabricated symmetrical DPA with a dimension of $105\ mm \times 65\ mm$ is shown in Fig. 14. The efficiency and gain performances are measured with a 10%-duty-cycle pulse excitation due to the heat effect caused by the high output power and the surface-mount package of the transistor.

TABLE 3. Comparison with recently reported DPAs.

Ref	Freq (GHz)	P_{sat} (dBm)	DE_{sat} (%)	OBO (dB)	DE_{low} (%)	Gain (dB)
[7]	3.4-3.5	49.5	58-62	6	46-50	8.6-9
[8]	1.7-2.6	44.6-46.3	57-66	6	47-57	10.2-11.6
[12]	1.7-2.8	44-44.5	57-71	6	50-55	12-14.5
[13]	2.2-3	39.5-41.5	50-67	6	36-48	6-8.6
[14]	3-3.6	43-44	55-66	6	38-56	8-11
This work	3.3-3.75	48-48.8	58-71	8	44-55	11.8-13.5

The measured DE and gain versus the output power are shown in Fig. 15 and Fig. 16, respectively. The DPA realizes good performances on efficiency and gain across the frequency band ranging from 3.3 GHz to 3.75 GHz. The DPA delivers a saturated power of 48-48.8 dBm with a DE of 58%-71%. At 8 dB OBO, a measured DE of 44%-55% is achieved with a gain of 11.8-13.5 dB.

A comparison with recently reported DPAs is given in Table 3. The proposed DPA presents a high output power at high frequencies. With a symmetrical architecture, the DPA extends the OBO to 8 dB, while its efficiency performance is still comparable with other state-of-the-art DPAs.

To evaluate the linearity of the DPA, the modulated signal measurement is performed. When driven by a 2-carrier 40-MHz LTE signal with 8 dB PAPR at 3.45 GHz, the DE of 53% at an average output power of 40.7 dBm is obtained with an adjacent channel leakage ratio (ACLR) lower than −30 dBc, as shown in Fig. 17.

VI. CONCLUSION

In this paper, a broadband DPA with high output power for the base station in 5G has been proposed. With a SHSN integrated into the OMN, the effect on the second harmonic component caused by the dynamic load modulation can be eliminated. Hence, the second harmonic termination is determined by the SHMN and can be transformed to the pure reactance to meet the requirement of the conventional class-J mode. Then, the DPA will work in the conventional class-J mode at the saturated power. At the low power, a modified class-J mode is presented to provide a wide impedance design space and extend the OBO to 8 dB with symmetrical architecture. Experimental results show the DPA delivers 48-48.8 dBm saturated power with a DE of 58%-71%. Meanwhile, at 8 dB OBO, a measured DE of 44%-55% is achieved with a gain of 11.8-13.5 dB across the frequency from 3.3 GHz to 3.75 GHz. A good linearity of −30 dBc ACLR is measured when driven by a 2-carrier 40-MHz LTE signal with 8 dB PAPR.

REFERENCES

[1] C.-X. Wang *et al.*, "Cellular architecture and key technologies for 5G wireless communication networks," *IEEE Commun. Mag.*, vol. 52, no. 2, pp. 122–130, Feb. 2014.

[2] F. Wang, A. H. Yang, D. F. Kimball, L. E. Larson, and P. M. Asbeck, "Design of wide-bandwidth envelope-tracking power amplifiers for OFDM applications," *IEEE Trans. Microw. Theory Techn.*, vol. 53, no. 4, pp. 1244–1255, Apr. 2005.

[3] W. H. Doherty, "A new high efficiency power amplifier for modulated waves," *Proc. Inst. Radio Eng.*, vol. 24, no. 9, pp. 1163–1182, Sep. 1936.

[4] D. Cox, "Linear amplification with nonlinear components," *IEEE Trans. Commun.*, vol. COM-22, no. 12, pp. 1942–1945, Dec. 1974.

[5] F. Wang *et al.*, "An improved power-added efficiency 19-dBm hybrid envelope elimination and restoration power amplifier for 802.11 g WLAN applications," *IEEE Trans. Microw. Theory Techn.*, vol. 54, no. 12, pp. 4086–4099, Dec. 2006.

[6] V. Camarchia, M. Pirola, R. Quaglia, S. Jee, Y. Cho, and B. Kim, "The Doherty power amplifier: Review of recent solutions and trends," *IEEE Trans. Microw. Theory Techn.*, vol. 63, no. 2, pp. 559–571, Feb. 2015.

[7] J. Xia, X. Zhu, L. Zhang, J. Zhai, and Y. Sun, "High-efficiency GaN Doherty power amplifier for 100-MHz LTE-advanced application based on modified load modulation network," *IEEE Trans. Microw. Theory Techn.*, vol. 61, no. 8, pp. 2911–2921, Aug. 2013.

[8] J. Pang, S. He, C. Huang, Z. Dai, J. Peng, and F. You, "A post-matching Doherty power amplifier employing low-order impedance inverters for broadband applications," *IEEE Trans. Microw. Theory Techn.*, vol. 63, no. 12, pp. 4061–4071, Dec. 2015.

[9] J. Pang, S. He, Z. Dai, C. Huang, J. Peng, and F. You, "Design of a post-matching asymmetric Doherty power amplifier for broadband applications," *IEEE Microw. Wireless Compon. Lett.*, vol. 26, no. 1, pp. 52–54, Jan. 2015.

[10] X. Chen and W. Chen, "A novel broadband Doherty power amplifier with post-matching structure," in *Proc. Asia–Pacific Microw. Conf.*, 2012, pp. 370–372.

[11] D. Gustafsson, C. M. Andersson, and C. Fager, "A modified Doherty power amplifier with extended bandwidth and reconfigurable efficiency," *IEEE Trans. Microw. Theory Techn.*, vol. 61, no. 1, pp. 533–542, Jan. 2013.

[12] J. Xia, M. Yang, Y. Guo, and A. Zhu, "A broadband high-efficiency Doherty power amplifier with integrated compensating reactance," *IEEE Trans. Microw. Theory Techn.*, vol. 64, no. 7, pp. 2014–2024, Jul. 2016.

[13] G. Sun and R. H. Jansen, "Broadband Doherty power amplifier via real frequency technique," *IEEE Trans. Microw. Theory Techn.*, vol. 60, no. 1, pp. 99–111, Jan. 2012.

[14] J. M. Rubio, J. Fang, V. Camarchia, R. Quaglia, M. Pirola, and G. Ghione, "3-3.6-GHz wideband GaN Doherty power amplifier exploiting output compensation stages," *IEEE Trans. Microw. Theory Techn.*, vol. 60, no. 8, pp. 2543–2548, Aug. 2012.

[15] P. Colantonio, F. Giannini, R. Giofre, and L. Piazzon, "Increasing Doherty amplifier average efficiency exploiting device knee voltage behavior," *IEEE Trans. Microw. Theory Techn.*, vol. 59, no. 9, pp. 2295–2305, Sep. 2011.

[16] R. Darraji and F. M. Ghannouchi, "Digital Doherty amplifier with enhanced efficiency and extended range," *IEEE Trans. Microw. Theory Techn.*, vol. 59, no. 11, pp. 2898–2909, Nov. 2011.

[17] S. Chen and Q. Xue, "Optimized load modulation network for Doherty power amplifier performance enhancement," *IEEE Trans. Microw. Theory Techn.*, vol. 60, no. 11, pp. 3474–3481, Nov. 2012.

[18] X. H. Fang and K.-M. M. Cheng, "Extension of high-efficiency range of Doherty amplifier by using complex combining load," *IEEE Trans. Microw. Theory Techn.*, vol. 62, no. 9, pp. 2038–2047, Sep. 2014.

[19] S. C. Cripps, *RF Power Amplifiers for Wireless Communications*, 2nd ed. Norwood, MA, USA: Artech House, 2006.

[20] Y. Y. Woo, Y. Yang, and B. Kim, "Analysis and experiments for high-efficiency class-F and inverse class-F power amplifiers," *IEEE Trans. Microw. Theory Techn.*, vol. 54, no. 5, pp. 1969–1974, May 2006.

[21] S. C. Cripps, P. J. Tasker, A. L. Clarke, J. Lees, and J. Benedikt, "On the continuity of high efficiency modes in linear RF power amplifiers," *IEEE Microw. Wireless Compon. Lett.*, vol. 19, no. 10, pp. 665–667, Oct. 2009.

[22] T. Canning, P. J. Tasker, and S. C. Cripps, "Continuous mode power amplifier design using harmonic clipping contours: Theory and practice," *IEEE Trans. Microw. Theory Techn.*, vol. 62, no. 1, pp. 100–110, Jan. 2014.

[23] V. Carrubba *et al.*, "On the extension of the continuous class-F mode power amplifier," *IEEE Trans. Microw. Theory Techn.*, vol. 59, no. 5, pp. 1294–1303, May 2011.

[24] W. Shi, S. He, and Q. Li, "A series of inverse continuous modes for designing broadband power amplifiers," *IEEE Microw. Wireless Compon. Lett.*, vol. 26, no. 7, pp. 525–527, Jul. 2016.

[25] K. Chen and D. Peroulis, "Design of broadband highly efficient harmonic-tuned power amplifier using in-band continuous Class-F^{-1}/F mode transferring," *IEEE Trans. Microw. Theory Techn.*, vol. 60, no. 12, pp. 4107–4116, Dec. 2012.
[26] Z. Lu and W. Chen, "Resistive second-harmonic impedance continuous class-F power amplifier with over one octave bandwidth for cognitive radios," *IEEE J. Emerging Sel. Topics Circuits Syst.*, vol. 3, no. 4, pp. 489–497, Dec. 2013.
[27] J. Rahola, "Power waves and conjugate matching," *IEEE Trans. Circuits Syst. II, Exp. Briefs*, vol. 55, no. 1, pp. 92–96, Jan. 2008.
[28] P. J. Tasker and J. Benedikt, "Waveform inspired models and the harmonic balance emulator," *IEEE Microw. Mag.*, vol. 12, no. 2, pp. 38–54, Apr. 2011.
[29] J. Pang, S. He, Z. Dai, C. Huang, J. Peng, and F. You, "Design of continuous-mode GaN power amplifier with compact fundamental impedance solutions on package plane," *IET Microw., Antennas Propag.*, vol. 10, no. 10, pp. 1056–1064, Jul. 2016.

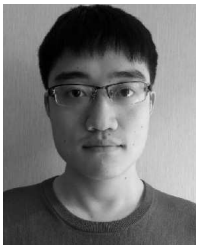

CHAOYI HUANG received the B.S. degree in electronic information engineering from the University of Electronic Science Technology of China (UESTC), Chengdu, China, in 2011, where he is currently pursuing the Ph.D. degree.

He is currently with the Smart Hybrid Radio Laboratory, UESTC. He is currently researching on design techniques for broadband high-efficiency and linear power amplifiers.

SONGBAI HE received the B.S., M.S., and Ph.D. degrees in electronic engineering from the University of Electronic Science and Technology of China (UESTC), Chengdu, China, in 1995, 1998, and 2003, respectively.

In 2004, he visited Chiba University, Japan, where he involved in the research of high-efficiency switch-mode power amplifiers. In 2005, he returned to UESTC, where he is currently a Professor. His research interests include RF/MW circuits and systems, frequency synthesis, wireless communication, and nonlinear dynamic systems.

FEI YOU received the bachelor's degree in electronic engineering and the Ph.D. degree in circuits and systems from the University of Electronic Science and Technology of China (UESTC) in 2004 and 2009, respectively. He is currently an Associate Professor with the School of Electronic Engineering, UESTC. From 2015 to 2016, he visited the High Frequency Center, Cardiff University, as an Academic Visitor.

His research interests include high-efficiency power amplifier design and its application in linearization transmitters. His current research plan is to build a digital polar transmitter for the broadband communication systems. The design method of the class-E power amplifier at microwave band, the high-efficiency broadband dc modulator, and the digital predistortion linearization method for the digital polar transmitter are the current key research points.